



CHALMERS
UNIVERSITY OF TECHNOLOGY

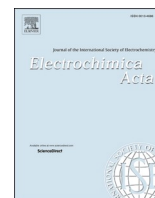
Ionic and Electronic Conductivity in Structural Negative Electrodes

Downloaded from: <https://research.chalmers.se>, 2025-02-19 14:51 UTC






Citation for the original published paper (version of record):

Pipertzis, A., Xu, J., Abdou, N. et al (2025). Ionic and Electronic Conductivity in Structural Negative Electrodes. *Electrochimica Acta*, 512. <http://dx.doi.org/10.1016/j.electacta.2024.145501>

N.B. When citing this work, cite the original published paper.



Ionic and electronic conductivity in structural negative electrodes

Achilleas Pipertzis^{a,*} , Johanna Xu^b , Nicole Abdou^c , Anna Martinelli^c, Leif.E. Asp^b ,
Jan Swenson^{a,*} 

^a Department of Physics, Chalmers University of Technology, 41296, Gothenburg, Sweden

^b Department of Industrial and Materials Science, Chalmers University of Technology, 41296, Gothenburg, Sweden

^c Department of Chemistry and Chemical Engineering, Chalmers University of Technology 41296, Gothenburg, Sweden

ARTICLE INFO

Keywords:

Ionic conductivity
Electrode laminas
Dielectric spectroscopy
Galvanostatic cycling
Lithiated/delithiated states

ABSTRACT

The concept of structural battery presents great potential for achieving substantial weight and volume reduction in electrified transportation. A unidirectional electrode lamina consists of carbon fibres embedded in a heterogeneous structural battery electrolyte. Dielectric spectroscopy measurements reveal the presence of both ionic and electronic conductivity through-the-thickness of electrode laminas. We report that the ionic conductivity, facilitated by the ions diffusing through the structural battery electrolyte, is reminiscent of that found in free-standing structural battery electrolytes and increases with a higher content of the ion-conducting phase. On the other hand, the through thickness electronic conductivity is dictated by the size of the electronically insulating electrolyte regions and the inter-fibre contact points forming the interconnected carbon fibre network. For suppressing the out-of-plane electronic conductivity and potential battery short-circuits in thin electrode laminas ($\leq 700 \mu\text{m}$) a glass-fibre separator is required. After galvanostatic cycling, we show that the fully-delithiated electrode lamina exhibits enhanced ionic conductivity. It indicates the presence of open microcracks, formed due the extensive expansion/contraction of carbon fibres upon charging/discharging. Our study provides valuable impedance and electrochemistry data in structural battery electrodes and half-cells, paving the way for the design of innovative, lightweight structural battery cells.

1. Introduction

The substantial mass of conventional batteries constitutes a notable drawback for their implementation in electrified transportation, by limiting the driving range and increasing the associated cost [1]. A promising mass-less energy storage system is commonly called a structural battery (SB) [2–5]. This innovative technology simultaneously integrates energy storage with structural robustness. This dual functionality results in substantial savings in both mass and volume, thereby facilitating the electrification of, for example, aircraft [6]. The research on SBs has recently gained significant interest with Tesla, for instance, adopting a structural battery concept in electric vehicles [7]. Nevertheless, the current challenge lies in the deficiency of high-performance electrodes and electrolytes, yielding lower energy and power densities when compared to commercial batteries.

Basically, the SB design is based on carbon fibre reinforced polymer composites, by combining the properties of traditional composite laminates and conventional Li-ion batteries. A structural negative electrode

lamina consists of carbon fibres (CFs) embedded in a bi-continuous Li-ion conductive electrolyte, denoted as structural battery electrolyte (SBE). Thus, this configuration results in a combination of high electrochemical and mechanical performance, yielding multifunctionality [2,3,6].

Heterogeneous SBEs comprise a solid porous polymer network and a liquid electrolyte in the pores of this network, providing mechanical stability and high ionic conductivity, respectively [8–12]. Such electrolytes are synthesized through a polymerization induced phase separation process, either initiated by ultraviolet (UV) or thermal methods [9,10]. Ihrner et al. [9] designed a promising methacrylate-based SBE using a UV-curing synthetic approach, which resulted in an elastic modulus of about 360 MPa and an ionic conductivity of $0.2 \text{ mS}\cdot\text{cm}^{-1}$, at ambient temperature. Subsequently, in a follow-up study by Schneider et al. [10], a thermal curing processing route was employed, resulting in SBEs with enhanced thermo-mechanical properties, reaching up to 750 MPa, while maintaining electrochemical performance comparable to UV-cured counterparts. In a previous study, we adopted the same

* Corresponding authors.

E-mail addresses: achilleas.pipertzis@chalmers.se (A. Pipertzis), jan.swenson@chalmers.se (J. Swenson).

<https://doi.org/10.1016/j.electacta.2024.145501>

Received 8 October 2024; Received in revised form 5 December 2024; Accepted 9 December 2024

Available online 10 December 2024

0013-4686/© 2024 The Author(s). Published by Elsevier Ltd. This is an open access article under the CC BY license (<http://creativecommons.org/licenses/by/4.0/>).

synthetic method for designing SBEs with the same “hard” phase and an ion-conducting phase that was based on a protic ionic liquid [11]. This material concept resulted in a good combination of ionic conductivity ($0.13 \text{ mS}\cdot\text{cm}^{-1}$) and mechanical stability (100 MPa), coupled with an exceptional thermal stability [11]. Notably, the synthesis method by thermal-curing proves advantageous for the fabrication of a full structural battery cell as well [10].

CFs play a significant role in providing mechanical reinforcement, Li-ion insertion, and high electronic conductivity in a SB. Moreover, they are semi-conductors, eliminating the need for current collectors, which further reduces the weight of the battery. Therefore, the multifunctionality of CFs is fundamental to the achievement of both structural stability and electrical functionality in SBEs.

Comprehensive investigations of mechanical and electrochemical performance of half and full SB cells have been carried out in previous studies [3,13–19]. It was evident that key factors such as the electrode thickness, the ionic conductivity of the SBE ($10^{-4} \text{ S}\cdot\text{cm}^{-1}$) and the applied current significantly affect the electrochemical performance [13]. Moreover, fibre electrode expansion and contraction were proven upon electrochemical cycling. The effect of cycling (state-of-charge) on the impedance of full battery cells has also been investigated [14,16]. Additionally, it was demonstrated that the temperature and applied tensile load during the stabilization/oxidation and carbonization stages of fibre manufacturing determines the microstructure, in turn influencing both the mechanical and electrochemical performance [15]. In the first-generation structural battery composites, Asp et al. [3] unveiled a structural battery composite cell featuring unprecedented multifunctional properties (24 Whkg^{-1} energy density and an elastic modulus of 26 GPa). In a subsequent work [16], SB cells with an energy density of 41.2 Whkg^{-1} (i.e. 75 % increase of electrochemical properties) while maintaining the mechanical robustness of the first-generation cells, were reported. Recently, the third-generation structural battery, the all-fibre SB, was demonstrated exhibiting an elastic modulus of 76 GPa and an energy density of 30 Whkg^{-1} [20]. It is noteworthy that existing literature highlights an inherent trade-off between tensile strength (mechanical) and electrochemical performance in multifunctional composite materials [3,5,6]. This trade-off needs to be taken into careful consideration during the design of novel-lightweight structural battery cells.

The SB electrode laminas (i.e. carbon-fibre reinforced SBE composites) can simultaneously provide electronic conduction (through the CFs), ionic conduction (facilitated by ions diffusing into the SBE) as well as structural stability (maintained by both CFs and SBE). In unidirectional laminas, CFs are oriented in parallel along one direction yielding a distinct anisotropy in electronic conductivity and mechanical properties along the fibre direction and in the thickness direction. The in-plane electronic conductivity is proportional to the volume fraction of the fibres and the conductivity value of the single fibres themselves. Conversely, the out-of-plane electronic conductivity is substantially lower due to the presence of the electronically insulating polymer matrix and the lower transversal conductivity of the fibres [21]. If a negligible out-of-plane electronic conductivity can be obtained without the use of a separator it is of great importance for designing novel SB cells since it further reduces the SB mass. Furthermore, the non-destructive evaluation of through-thickness electronic conductivity is essential for acquiring information about safety factors, such as delamination due to impacts and fatigue loads on carbon fibre reinforced polymers, and for assessing damage incurred during both the production process and operational use [22]. It also contributes to the development of effective protection against lightning strikes for SBs in aircraft and automotive.

Herein, we have used dielectric spectroscopy to study the mixed ionic and electronic conduction in unidirectional electrode laminas. The SBE is composed of a glassy phase of ethoxylated Bisphenol A dimethacrylate and a liquid ion-conducting phase based on a mixture of organic carbonate solvents doped with Li-salt. The dielectric measurements reveal a combination of ionic and out-of-plane electronic

conductivity, experimentally verifying the multifunctionality of the SBs. The factors that dictate the ionic and the through-thickness electronic conductivity were studied. Moreover, we report on the effect of galvanostatic cycling on the ionic conductivity of unidirectional electrode laminas.

2. Materials and methods

2.1. Free-standing SBEs

The two-phase bi-continuous SBE consists of a polymeric material and liquid electrolyte. Ethoxylated Bisphenol A dimethacrylate (EBPADMA, $M_w = 540 \text{ g}\cdot\text{mol}^{-1}$) monomer was provided by Sartomer (Arkema Group). The thermal initiator 2,2'-azobis(2-methylpropionitrile) (AIBN), the lithium bis(tri-fluoromethane)sulfonimide (LiTFSI) salt, and the organic carbonate solvents ethylene carbonate (EC) (battery grade $\geq 99 \%$, acid $< 10 \text{ ppm}$, $\text{H}_2\text{O} < 10 \text{ ppm}$) and propylene carbonate (PC) (battery grade $\geq 99 \%$, acid $< 10 \text{ ppm}$, $\text{H}_2\text{O} < 10 \text{ ppm}$) were purchased from Sigma Aldrich and used as received. The chemical structure of the employed compounds is depicted in Fig. S1 of the Supplementary Information (SI). The liquid electrolyte contains 1.0 M LiTFSI dissolved in EC and PC (50:50 wt.%). The SBE solution is a mixture of liquid electrolyte, the monomer and thermal initiator. The amount of liquid electrolyte in the SBE is varied, denoted as SBE $_y$, where y indicates the weight fraction of the liquid electrolyte. All samples with SBE were prepared in a glovebox filled with dry argon ($< 1 \text{ ppm}$ of H_2O , $< 1 \text{ ppm}$ of O_2) and thermally cured at $90 \text{ }^\circ\text{C}$ (363 K) for 45 min. The temperature dependence of the ionic conductivity as well as the factors that dictate the ion conduction in free-standing SBEs are discussed in detail in SI in relation to Fig. S2, Fig. S3 and Table S1.

2.2. Electrode laminas

Carbon fibre structural electrodes were prepared using two methods: vacuum infusion for thin laminas and a combination of vacuum infusion and hand-layup for thick laminas. For the electrode preparation, two layers of unidirectional T800SC-12k-50C PAN-based CF tows (15 mm width, $0.52 \text{ g}\cdot\text{m}^{-1}$ linear tow weight), supplied by Oxeon AB, Sweden, were used. A copper foil strip was adhered to the CFs using a conductive silver paint. The CFs were then covered with a release film and a polyester felt cloth to act as a distribution medium. The assembly was sealed using a vacuum bag and rubber tape and dried in a vacuum oven at $50 \text{ }^\circ\text{C}$ for 12 h. The SBE solution was prepared in a glovebox under a dry argon atmosphere ($< 1 \text{ ppm}$ H_2O , $< 1 \text{ ppm}$ O_2), as described in the “Free Standing SBEs” section. The solution container was sealed, and the vacuum infusion of the prepared CF tow assembly was performed outside the glovebox.

For the synthesis of thick laminas ($\sim 700 \mu\text{m}$), the entire process was conducted inside a glovebox under a dry argon atmosphere ($< 1 \text{ ppm}$ H_2O , $< 1 \text{ ppm}$ O_2) to maintain controlled conditions. The synthesis followed a two-step procedure: first, the electrode lamina was fabricated using vacuum infusion and curing. This cured lamina was then placed in a mold with spacing material to control the thickness of the bulk SBE face sheets. Subsequently, the SBE solution was added dropwise (using a pipette) to fill the mold, ensuring a uniform final laminate thickness.

To study the effect of cycling on the ionic and out-of-plane electronic conductivity, specimens were manufactured with a separator (Whatman glass-microfibre filter, Whatman GF/A, $260 \mu\text{m}$, supplied by Sigma Aldrich) on both sides of the CF layers. After a second thermal curing at $90 \text{ }^\circ\text{C}$ (363 K) for 45 min, the CF lamina was removed from the vacuum bag inside the glovebox and directly inserted into a two-electrode pouch cell. Lithium metal foil served as the counter and reference electrode, with a nickel current collector.

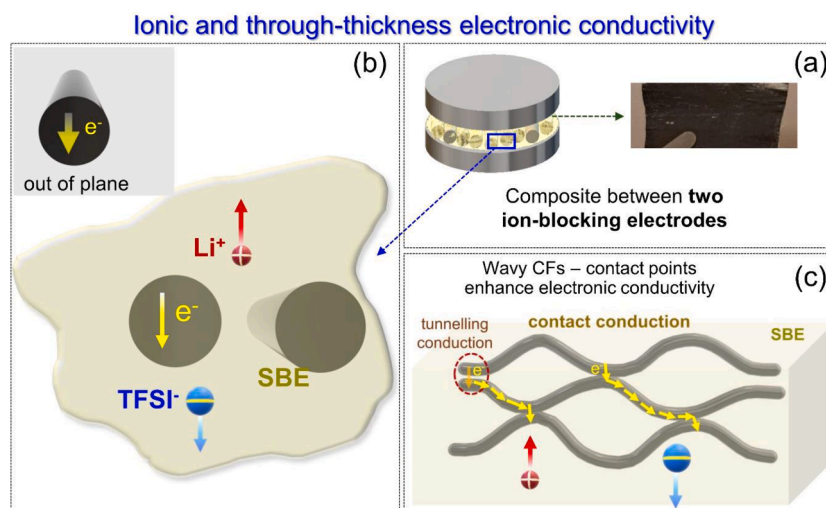


Fig. 1. Schematic representation of (a) the dielectric capacitor, the transport of ions and the through-thickness electronic conductivity and (c) the wavy nature of CFs and the contact points along with the tunneling effect that enhance the through-thickness electronic conductivity.

2.3. Dielectric spectroscopy

Dielectric spectroscopy measurements were performed using a Novocontrol GmbH broadband dielectric spectrometer, covering the frequency range from 10^{-2} to 10^7 Hz. Dielectric spectroscopy can be used for determining (i) the ionic conductivity in free-standing films of SBEs and (ii) the separation of electronic and ionic conductivity components in mixed conductors and composite systems. The samples were placed between two ion-blocking (stainless-steel) electrodes with 5 mm or 10 mm diameter. The diameter and thickness of electrodes and samples were measured with a Mitutoyo absolute digital caliper. Measurements were conducted in a temperature range between 173 K and 393 K in steps of 5 K, with a stabilization time of 600 s at each temperature. The temperature was controlled using a nitrogen gas cryostat, with a stability of ± 0.1 K. The experimental impedance data were modelled by an equivalent circuit and these data were thereafter fitted by a complex non-linear least squares fitting procedure using the Zsim and WinFit (provided by Novocontrol) software packages. It should be noted that the instrument's resolution decreases at frequencies higher than 2 MHz, and therefore some inconsistent impedance data in the frequency range between 2 MHz and 10 MHz have been omitted from the fitting

procedure. A 2-electrode cell, using symmetric ion-blocking electrodes was employed for the measurements of both the free-standing polymer membranes and electrode composite laminas (see Fig. 1a). A 3- or 4-electrode cell is required for investigating the interfacial regions between the CFs and the SBE. The existence of contact points between adjacent fibres enables the out-of-plane electronic conduction, which is non-negligible even in the presence of the electronically-insulating polymer matrix, elaborated upon below. These inter-fibre contact points have been demonstrated in previous studies through Scanning Electron Microscopy (SEM) images [13].

2.4. Galvanostatic cycling

The assembled half-cells were cycled between 0.01 V and 1.5 V vs. Li/Li⁺ for 10 complete galvanostatic charge/discharge cycles for pre-conditioning at ambient temperature, using a Neware CT-4008-5V10mA-164 battery cycler. The applied current density was $32.1 \text{ mA}\cdot\text{g}^{-1}$, corresponding to approximately 0.1 C, based on theoretical capacity for graphite. Following preconditioning, the cells were either potentiostatically discharged or charged for full lithiation and delithiation, respectively.

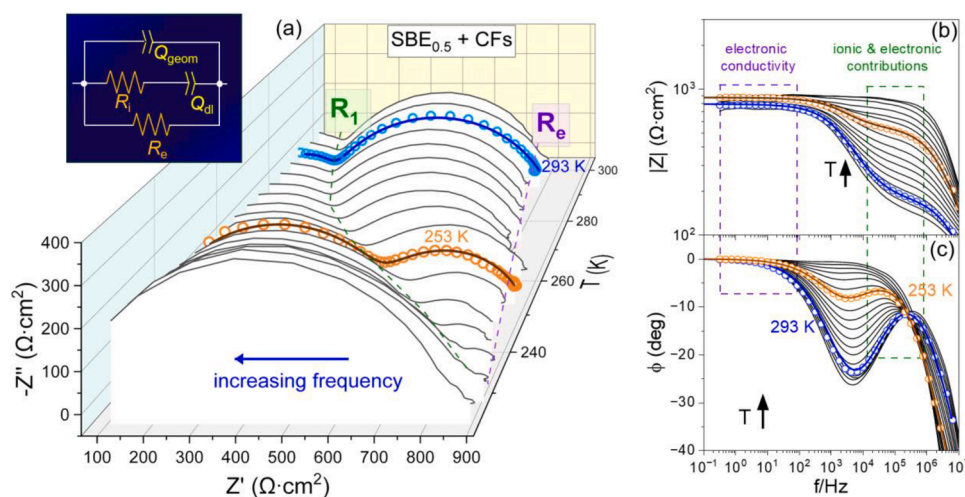


Fig. 2. (a) Nyquist plot and (b,c) Bode plots of the SBE_{0.5}+CFs composite with sample thickness equal to $170 \mu\text{m}$, across the temperature range from 223 K to 303 K, in steps of 5 K. The inset in (a) represents the equivalent circuit used to simulate the electrochemical data. Fitting simulations (coloured lines) are provided at two temperatures: $T = 253 \text{ K}$ (orange) and $T = 293 \text{ K}$ (blue), where the symbols correspond to the measured data.

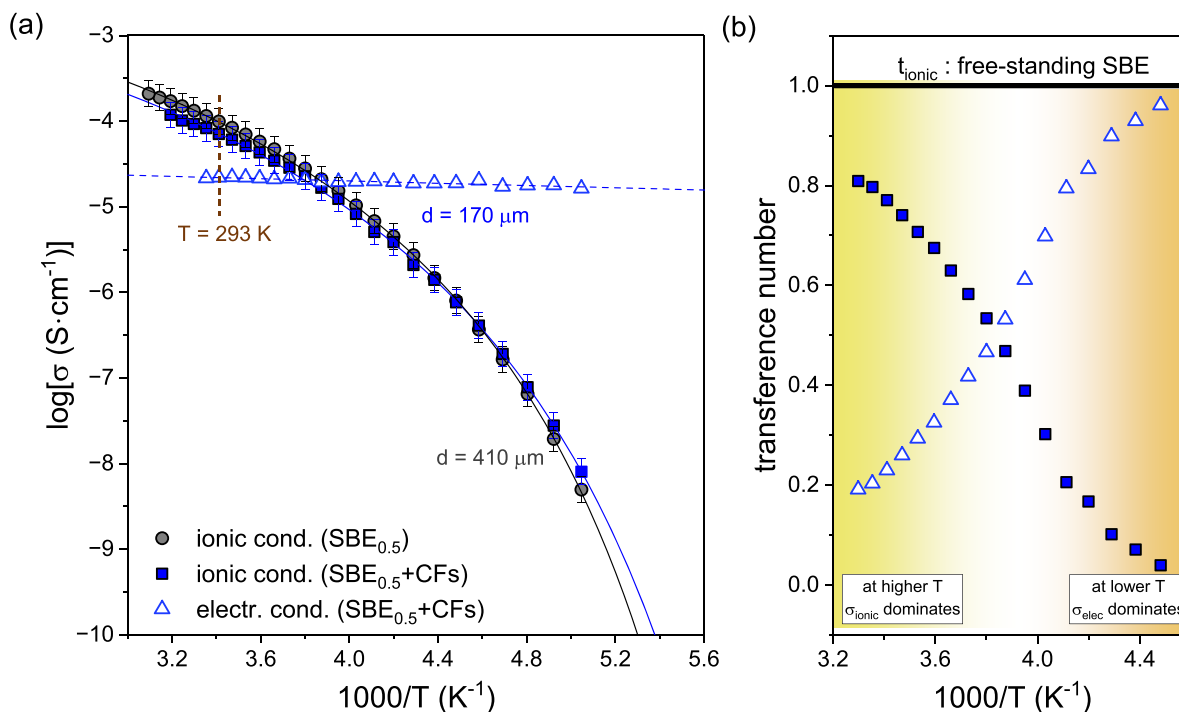


Fig. 3. (a) Inverse temperature dependence of ionic (filled symbols) and electronic (open symbols) conductivity for the SBE_{0.5}+CFs (blue symbols) and its respective free-standing SBE film (circle symbols), upon heating. The solid and dashed lines represent fits to Eq. (3) and Eq. (4), respectively. The sample thicknesses are 410 μm and 170 μm for the free-standing SBE and the respective electrode lamina, as indicated. The error bars were extracted by measuring three different samples. (b) Transference numbers associated with the ionic (filled symbols) and electronic (open symbols) transport, calculated from Eqs. (5) and (6), respectively.

3. Results and discussion

3.1. Ionic and through-thickness electronic conductivity in SB electrode laminae

Quantitative insight into the ionic and the out-of-plane electronic conductivity in SB electrode laminae has been achieved by dielectric spectroscopy [23]. The Nyquist and Bode plots of the carbon fibre reinforced polymer composites labelled SBE_{0.5}+CFs and SBE_{0.7}+CFs, are presented in Fig. 2 and Fig. S4, respectively.

The Nyquist plot of the composite system (SBE+CFs) reveals the presence of two semicircles, reflecting the combined contribution of ion and electron transport. R_1 is the intersection point (where the imaginary part of the impedance Z'' approaches zero) and is associated with the ionic resistance (R_i) and electronic resistance (R_e), through the following equation:

$$\frac{1}{R_1} = \frac{1}{R_i} + \frac{1}{R_e} \Leftrightarrow R_1 = \frac{R_i R_e}{R_i + R_e} \Leftrightarrow R_i = \frac{R_1 R_e}{R_e - R_1} \quad (1)$$

The total radius of the two semicircles reflects the electronic resistance. It is worth noting that at lower temperatures, the low frequency tail observed in purely ionic conductors is hidden by the electronic contribution. This clearly indicates the presence of pathways for the transport of electronic charge [23–24]. Complementary insights can be obtained from the Bode plots, depicting the frequency-dependent modulus of impedance, defined as $Z = \sqrt{Z'^2 + Z''^2}$ and the phase angle, defined as $\phi = \tan^{-1}\left(\frac{Z''}{Z'}\right)$ (see Fig. 2(b,c)), where Z' is the real part of the impedance. These figures show that the modulus of impedance and phase angle in the composite system exhibit two distinct processes, evidenced as plateaus and peaks, respectively. Moreover, the mixed conduction can be verified from the two plateaus in the real part of the complex conductivity (i.e. conductivity plot, see Fig. S5). A comparison between the impedance data of the electrode laminae and

the free-standing polymer membranes is provided in Fig. S6–S8 of SI, after normalization with cross-sectional electrode area. Therefore, within electrode laminae, electron transport occurs between the ion-blocking electrodes, in addition to the ion transport of free-standing SBEs.

Representative fit simulations of the impedance data are provided in Fig. 2, at two distinct temperatures. The fitting of the two semicircles was achieved by employing the equivalent circuit presented in the inset of Fig. 2(a), as proposed by Huggins for mixed conductors [23]. It has an additional R_e connected in parallel arrangement with R_i , when compared to the one commonly employed for ion conducting electrolytes, as clearly depicted in Fig. S6(a,b). Instead of ideal capacitors, constant phase elements, CPEs, (i.e. non ideal capacitors) were employed. The impedance of a CPE is given by $Z_{CPE} = \frac{1}{(j\omega)^\alpha C}$, where α ranges from 0 to 1 and describes the capacitive behaviour. The double layer CPE characterizes the interfacial capacitances ($\sim \mu\text{F}$) between the composite material and ion-blocking electrodes [23,25]. Conversely, the geometric CPE ($\sim \text{pF}$) is associated with the material's dielectric constant. The values of the electrochemical parameters extracted from modelling of the impedance data are provided in Fig. S7–S9 of SI, for the investigated specimens.

The values of the ionic, σ_{ionic} and electronic, $\sigma_{\text{electronic}}$, conductivity can be calculated using the impedance data, through the following equation:

$$\sigma_{\text{ionic, electronic}} = d / (R_{i,e} \cdot A) \quad (2)$$

where d is the sample thickness, A is the electrolyte area between the lower and upper ion-blocking electrode, R_i and R_e are the ionic and electronic resistance extracted from modelling with the equivalent circuit. Alternatively, the conductivity values can be obtained from the plateaus in the real part of the complex conductivity, as illustrated in Fig. S5. However, for mixed conductors, the high-frequency plateau is related to the R_1 resistance (Eq. (1)), and not with R_i as it is the case for purely ionic conductors.

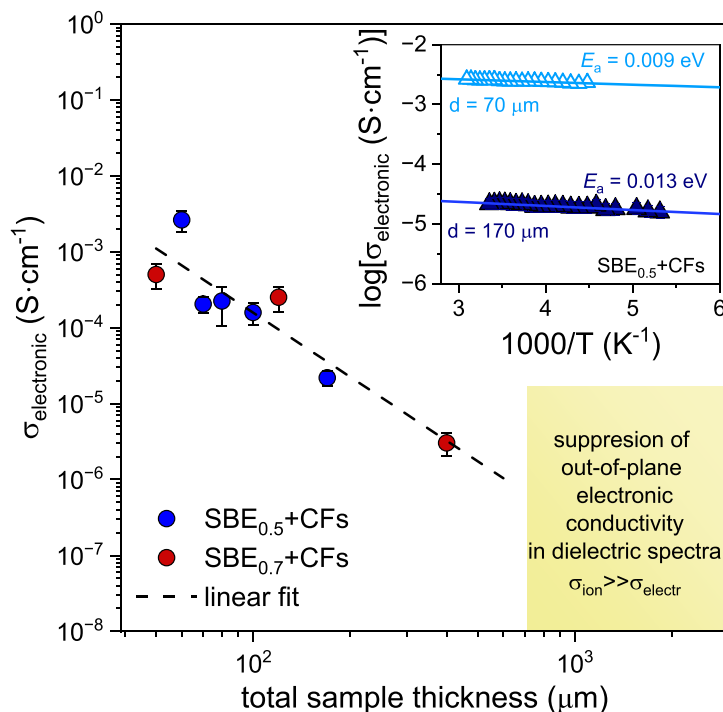


Fig. 4. Variation of electronic conductivity with total sample thickness for the SBE+CFs electrode laminas plotted in a log-log representation. The different colors represent different SBE compositions with; 0.5 wt. (blue symbols) and 0.7 wt. (red symbols) of the liquid electrolyte. The dashed line represents linear fit to the experimental data. Inset: Temperature dependence of electronic conductivity for two SBE_{0.5}+CFs electrode laminas with different thicknesses; 70 μm (cyan open triangles) and 170 μm (navy filled triangles). The solid lines represent fits by Eq. (4). The respective activation energies are provided. The electrode laminas (half-battery cells) were fabricated following the procedure described in the “Materials and Methods” section, for thin electrode samples with thickness, $d < 700$ μm. Each electrode sample consists of two layers of carbon fibers. The electronic conductivities were extracted using a two-electrode cell configuration. The reported total sample thickness refers to the thickness of each electrode lamina, measured with a Mitutoyo absolute digital caliper, excluding the presence of working electrodes.

The conductivity values are graphically presented as a function of inverse temperature and compared with those observed for free-standing polymer membranes, as illustrated in Fig. 3.

Fig. 3 shows that the presence of CFs does not markedly impact the ionic conductivity, which closely mirrors that found in free-standing SBEs. The ionic conductivity can be increased by increasing the content of the ion-conducting phase, aligning with the trend observed in free-standing polymer membranes (see Fig. S10). Specifically, the SBE_{0.5} film with and without CFs exhibit an ionic conductivity of approximately 0.2 mS·cm⁻¹. Additionally, the temperature dependence of the ionic conductivity is unaffected by the incorporation of CFs, and it can be described by the Vogel-Fulcher-Tammann (VFT) equation:

$$\sigma_{\text{ionic}}(T) = \sigma_0 \exp\left(-\frac{DT_0}{T - T_0}\right) \quad (3)$$

where, σ_0 is the dc-conductivity in the limit of very high temperatures, D is a parameter related to the deviation from an Arrhenius temperature dependent activation energy and T_0 is the “ideal” glass transition temperature, where the conductivity approaches zero. The VFT parameters are summarized in Table S2. On the other hand, the electronic conductivity exhibits a distinctly weaker temperature dependence, following the Arrhenius equation:

$$\sigma_{\text{electronic}}(T) = \sigma_0^e \exp\left(-\frac{E_a}{RT}\right) \quad (4)$$

where σ_0^e is the electronic conductivity at high temperatures, R is the gas constant and, E_a is the temperature independent activation energy, which obtains a value of 0.013 eV, for an electrode lamina with sample thickness 170 μm. The low activation energy of the electronic conductivity reflects the low energy required for the electrons to jump from one CF to another. This activation phenomenon is common for the electronic

conduction in composite materials with an insulating polymer matrix and conductive fillers (particles or fibres) [26].

The transference number of the ionic and the electronic conduction can be extracted from the following equations:

$$t_{\text{ionic}} = \frac{R_e - R_1}{R_e} \quad (5)$$

$$t_{\text{electronic}} = \frac{R_1}{R_e} \quad (6)$$

by employing the intersection resistances with the real axis. As illustrated in Fig. 3b, the ionic conductivity dominates at higher temperatures and the electronic conductivity at lower temperatures, as a consequence of their different temperature dependence.

Fig. 4 presents the dependence of the through-thickness electronic conductivity on the total sample thickness, for the electrode laminas bearing SBE with different compositions.

Specifically, the electronic conductivity decreases linearly, by increasing the total sample thickness in a log-log representation. A smaller composite thickness gives rise to a higher electronic conductivity, due to more contact points between the wavy CFs and the formation of a percolating network, facilitating the through-thickness transport of electrons, as depicted in the schematic representation of Fig. S11. Specifically, we can discern three characteristic thickness regions: (i) for $d \leq 70$ μm $\sigma_{\text{electronic}} \gg \sigma_{\text{ionic}}$, (ii) for $100 \leq d \leq 400$ μm $\sigma_{\text{electronic}} \approx \sigma_{\text{ionic}}$ and (iii) for $d \geq 700$ μm $\sigma_{\text{ionic}} \gg \sigma_{\text{electronic}}$. Particularly, when $d \leq 70$ μm, the electronic conductivity surpasses the ionic conductivity at the whole investigated temperature range, even for the high-conductivity SBE_{0.7}+CFs electrode. In the intermediate thickness regime, the electronic conductivity either matches or is lower than the ionic conductivity, thereby manifesting both types of conductivity in the dielectric spectra (see Fig. 2 and Fig. 3a). Thus, the through-thickness

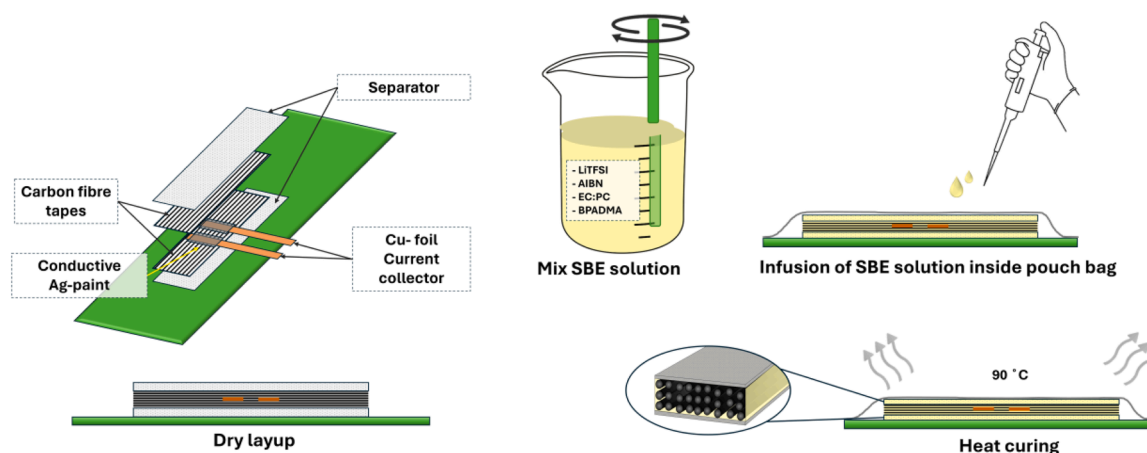


Fig. 5. Manufacture of the structural electrode laminas, dry layup of the CF layers with separator on both sides, preparation and impregnation of SBE followed by heat cure at 363 K.

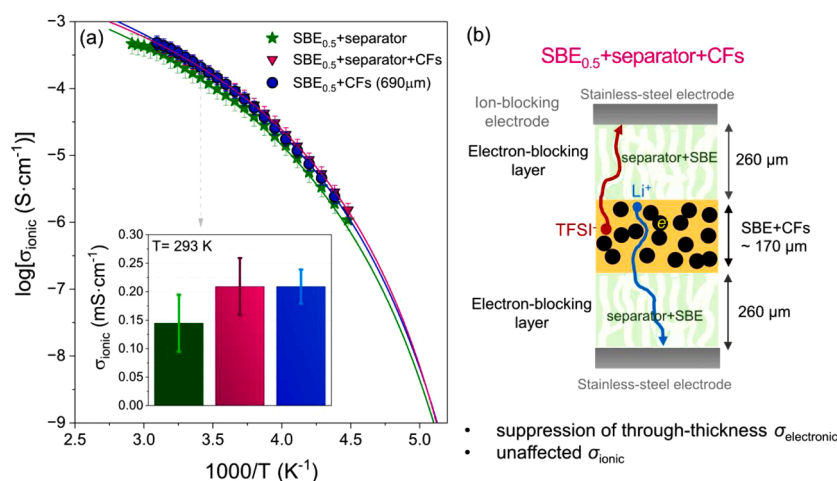


Fig. 6. (a) Extracted ionic conductivity values as a function of reciprocal temperature for the SBE_{0.5}+separator (green stars) and SBE_{0.5}+separator+CFs (magenta down-triangles) and SBE_{0.5}+CFs (blue circles), with sample thickness equal to 310 μm, 680 μm and 690 μm, respectively. The SBE_{0.5}+separator sample is composed of one separator layer combined with SBE at the same region. The reduced thickness can possibly account for the slightly reduced ionic conductivity. The lines represent fits by Eq. (3). The values of the ionic conductivity at 293 K are also shown in the inset. The error bars were extracted by measuring three different regions of the films. (b) An illustration of the SBE containing both separator and CFs.

electronic conductivity is primarily influenced by the size of the insulating polymer regions (i.e. the sample thickness) and the undulated nature of CFs (i.e. the synthesis), which determines whether contact points occur between the CFs. It implies that for thin SB electrode laminas ($\approx 200 \mu\text{m}$) with reduced mass and volume and increased electrochemical properties, an electronically insulating separator is required for preventing battery short-circuits.

3.2. Structural battery half-cells – suppression of through-thickness electronic conductivity

To suppress the through-thickness electronic conductivity and to study the effect of cycling on the ionic and out-of-plane electronic conductivity, specimens were manufactured with a separator (Whatman glass-microfibre filter, Whatman GF/A, 260 μm, supplied by Sigma Aldrich) on both sides of the CF layers. After a second thermal curing at 363 K (90 °C) for 45 min, the CF lamina was removed from the vacuum bag inside the glovebox and directly inserted into a two-electrode pouch cell. Lithium metal foil served as the counter and reference electrode, with a nickel current collector. The manufacture of SB half-cells is schematically illustrated in Fig. 5.

The separators must possess chemical stability with the electrolyte and electrode materials, alongside exhibiting excellent wettability, robust mechanical properties, thermal stability and high porosity facilitating ion transport. [27,28] The effect of the separator on the ionic conductivity of electrode laminas bearing separator layers is shown in Fig. 6 and compared with the ionic conductivity of the thick SBE_{0.5}+CFs specimen.

Anticipatedly, we exclusively observe the ionic conductivity plateau and one semi-circle in the conductivity and Nyquist plots (see Fig. S12), implying that the electronically insulating separator layers suppress the through-thickness electronic conductivity. It is worth noting that the ionic conductivity remains inside the experimental error when the separator layer is introduced and follows a similar VFT temperature dependence (see Table S3). At this point an obvious question that arises is how the electrochemical cycling affects the observed ionic conductivity in thin electrode laminas.

3.3. Effect of galvanostatic cycling on the ionic conductivity of SB half-cells

To study the effect of cycling on the ionic conduction of SB-half-cells,

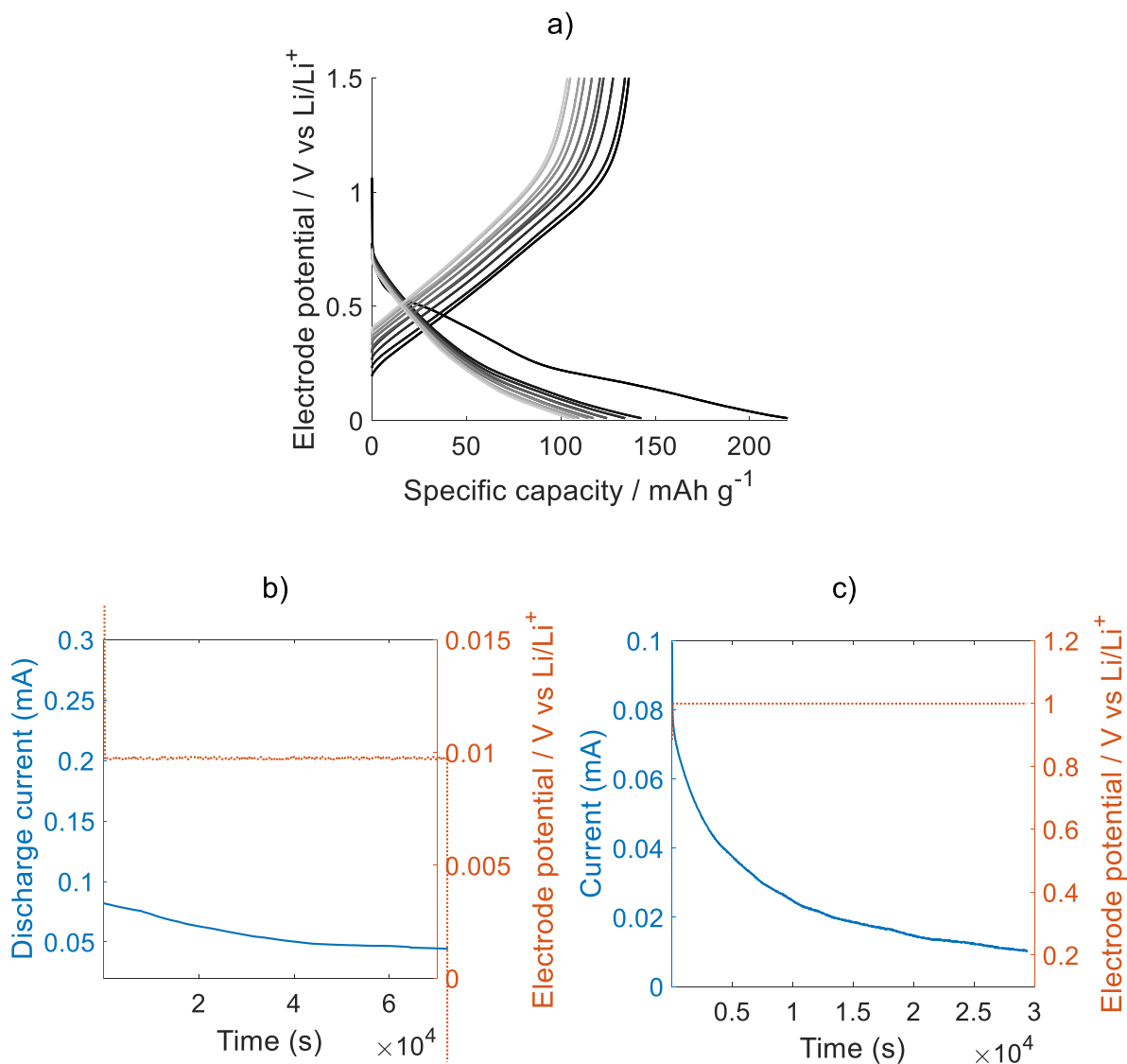


Fig. 7. (a) Ten initial galvanostatic charge/discharge cycles for CFs in SBE vs Li metal, followed by either (b) potentiostatic lithiation (discharge) and (c) potentiostatic delithiation (charge).

galvanostatic and potentiostatic cycling were performed in electrode laminas vs Li metal, and the results can be discussed with respect to Fig. 7.

Immediately after cycling, dielectric measurements were performed on the pristine, fully-lithiated, and fully-delithiated samples. The effect of cycling on the ionic conductivity is shown in Fig. 8.

Duan et al. [29] studied the volume expansion of the CFs in the pristine, lithiated, and delithiated states. The study found that lithiation of CFs resulted in a significant increase in cross-sectional area, indicating large volume expansion. The average cross-sectional area expanded by approximately 13.7 % in the liquid electrolyte. Furthermore, Carlstedt et al. [13] utilized in-situ video microscopy to study the fibre expansion during lithiation in both liquid electrolyte and SBE. The reversible longitudinal expansion was found to be approximately 0.8 % in the liquid electrolyte and 0.6 % in the SBE. The reduction in elongation for fibres in the SBE compared to the sample in the liquid electrolyte was attributed to the reduced specific capacity, rather than the constraining effect in the SBE.

Larsson et al. [30] developed a computational model considering finite strains and lithium concentration-dependent fibre moduli. The computational model was used to investigate the effect of lithium insertion in CFs on the internal stress state of the electrode in both fully

constrained and unconstrained cases, representing upper and lower bounds. The stress distributions showed levels higher than what can be expected for the strength of a glassy polymer. The constraints on the laminate on which the dielectric measurements in the present study are carried out lie between fully constrained and free expansion. Therefore, it is plausible that charging and discharging result in the formation of microdamage in the SBE. Such microdamage has a negative impact on the mechanical properties of the laminate in a direction transverse to the fibre orientation. The presence of microcracks provides a plausible explanation for the observed differences in ionic conductivity among the three different charge states. As the fibres are lithiated and microcracks have formed, the ionic conductivity remains similar to that of the pristine laminate, as the formed cracks are closed. However, as the fibres are delithiated, desertion of lithium causes the fibres to shrink back to the same dimensions as that of the pristine fibres, leaving the formed cracks open and changing the tortuosity of the SBE, which allows for higher ion transfer. Hence, the delithiated sample exhibits slightly higher values of ionic conductivity, compared to the pristine sample (see Fig. 8 and Fig. S13). The temperature dependence of the ionic conductivity follows Eq. (3), and the parameters are summarized in Table S4. The increase of the ionic conductivity can be regarded as an indirect verification of the presence of microdamages, following the expansion and contraction of

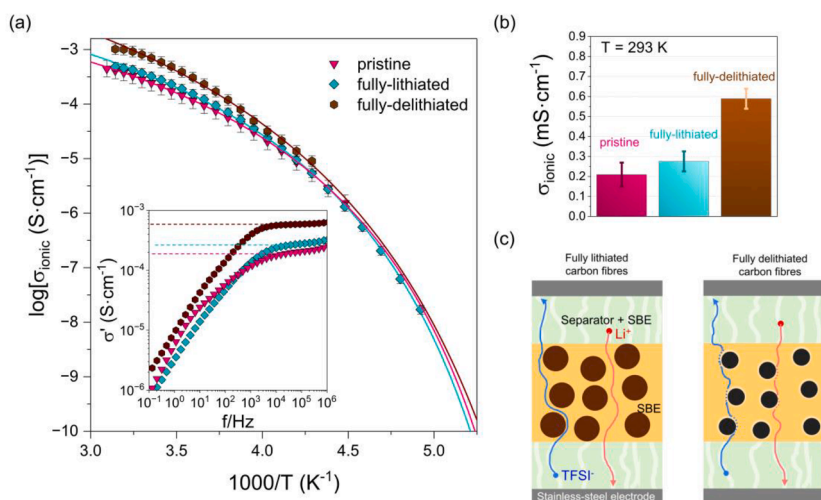


Fig. 8. Inverse temperature dependence of ionic conductivity for the SBE+separator+CFs composite systems; pristine (magenta up-triangles), fully-lithiated (green rhombi) and fully-delithiated (brown hexagons), with sample thickness equal to 680 μm , 570 μm and 610 μm , respectively. The error bars were calculated by measuring two different regions of the films. Inset. Real part of complex conductivity as a function of frequency. (b) Ionic conductivity values at ambient temperature. (c) Schematic representation of the fully-lithiated and the fully-delithiated states. It can be seen that the fully-delithiated sample exhibits increased ionic conductivity compared to the fully-lithiated and pristine samples.

CFs upon cycling.

4. Conclusions

Unidirectional electrode laminas, concurrently exhibiting electronic and ionic conductivity, were systematically investigated by means of dielectric spectroscopy. The ionic conductivity stems from long-range translational ion diffusion in the ion-conducting (i.e. liquid) phase of the heterogeneous SBE. It was evident that the incorporation of CFs does not affect the ionic conductivity, but it imparts electronic conductivity to the composite system. A two-electrode cell with symmetric ion-blocking electrodes was used for estimating the ionic conductivity and the through-thickness electronic conductivity. Notably, we highlight that the electronically insulating regions of the polymer matrix (which increases with the total sample thickness) and the inter-fibre-contact points (i.e. due to the wavy CFs), forming a percolating network are the primary factors dictating the through-thickness electronic conductivity. Hence, to prevent short-circuits, it is necessary to design either thick electrode laminas ($\geq 700 \mu\text{m}$) or thin electrode laminas ($\leq 200 \mu\text{m}$) with an electronically-insulating separator. It is important to note that the incorporation of a porous glass-fibre separator layers has a negligible impact on the ion transport properties.

Subsequently, the effect of electrochemical cycling on the ionic conductivity of a thin electrode lamina bearing glass-fibre separators was studied. An increased ionic conductivity, compared to the pristine laminate, was observed for the fully-delithiated sample. It reflects changes in the tortuosity of the SBE, caused by the presence of open microdamages (possibly filled with liquid electrolyte), formed upon the expansion/contraction of the CFs during cycling. To sum up, the results of this study provide crucial guidelines for the design of novel lightweight structural battery cells.

CRedit authorship contribution statement

Achilleas Pipertzis: Writing – review & editing, Writing – original draft, Visualization, Methodology, Investigation, Formal analysis, Data curation, Conceptualization. **Johanna Xu:** Writing – review & editing, Visualization, Resources, Methodology, Investigation, Data curation, Conceptualization. **Nicole Abdou:** Writing – review & editing, Visualization, Resources. **Anna Martinelli:** Writing – review & editing, Supervision, Funding acquisition. **Leif.E. Asp:** Writing – review & editing,

Supervision, Funding acquisition, Conceptualization. **Jan Swenson:** Writing – review & editing, Supervision, Project administration, Funding acquisition, Conceptualization.

Declaration of competing interest

The authors declare that they have no known competing financial interests or personal relationships that could have appeared to influence the work reported in this paper.

Acknowledgements

(AP, NA, AM, JS) were funded by a grant from the Area of Advance Materials Science at Chalmers University of Technology. (JX, LA) Funding from 2D TECH VINNOVA Competence center (Ref. 2019-00068) USAF, EOARD Award No. FA8655-21-1-7038, and ONR, USA, Award No. N62909-22-1-2037 is gratefully acknowledged.

Supplementary materials

Supplementary material associated with this article can be found, in the online version, at [doi:10.1016/j.electacta.2024.145501](https://doi.org/10.1016/j.electacta.2024.145501).

Data availability

Data will be made available on request.

References

- [1] J.-M. Tarascon, M. Armand, Issues and challenges facing rechargeable lithium batteries, *Nature* 414 (6861) (2001) 359–367.
- [2] L.E. Asp, M. Johansson, G. Lindbergh, J. Xu, D. Zenkert, Structural battery composites: a review, *Funct. Compos. Mater.* 1 (4) (2019) 042001.
- [3] L.E. Asp, K. Bouton, D. Carlstedt, S. Duan, R. Harnden, W. Johansson, M. Johansen, M.K. Johansson, G. Lindbergh, F. Liu, K. Pevuot, L.M. Schneider, J. Xu, D. Zenkert, A structural battery and its multifunctional performance, *Adv. Energ. Sust. Res.* 2 (3) (2021) 2000093.
- [4] G.J.H. Lim, K.K. Chan, N.A.A. Sutrisnoh, M. Srinivasan, Design of structural batteries: carbon fibers and alternative form factors, *Mater. Today Sustain.* 20 (2022) 100252.
- [5] J.L. Lutkenhaus, P. Flouda, Structural batteries take a load off, *Sci. Robot.* 5 (45) (2020) eabd7026.
- [6] A. Ishfaq, S.N. Nguyen, E.S. Greenhalgh, M.S. Shaffer, A.R. Kucernak, L.E. Asp, D. Zenkert, P. Linde, Multifunctional design, feasibility and requirements for

- structural power composites in future electric air taxis, *J. Compos. Mater.* 57 (4) (2023) 817–827.
- [7] C. Bos, Tesla's new structural battery pack—It's not cell-to-pack, it's cell-to-body, *CleanTechnica* 11 (2020).
- [8] J.F. Snyder, R.H. Carter, E.D. Wetzel, Electrochemical and mechanical behavior in mechanically robust solid polymer electrolytes for use in multifunctional structural batteries, *Chem. Mater.* 19 (15) (2007) 3793–3801.
- [9] N. Ihrner, W. Johannisson, F. Sieland, D. Zenkert, M. Johansson, Structural lithium ion battery electrolytes via reaction induced phase-separation, *J. Mat. Chem. A* 5 (48) (2017) 25652–25659.
- [10] L.M. Schneider, N. Ihrner, D. Zenkert, M. Johansson, Bicontinuous electrolytes via thermally initiated polymerization for structural Lithium ion batteries, *ACS Appl. Energy Mater.* 2 (6) (2019) 4362–4369.
- [11] A. Pipertzis, N. Abdou, J. Xu, L.E. Asp, A. Martinelli, J. Swenson, Ion transport, mechanical properties and relaxation dynamics in structural battery electrolytes consisting of an imidazolium protic ionic liquid confined into a methacrylate polymer, *Energy. Mater.* 3 (2023) 300050.
- [12] R. Tavano, M. Spagnol, N. Al-Rahimi, R. Joffe, J. Xu, L.E. Asp, Mechanical characterization of a structural battery electrolyte, *Polymer (Guildf)* 312 (2024) 127646.
- [13] D. Carlstedt, F. Rittweger, K. Runesson, A.M. Navarro-Suarez, J. Xu, S. Duan, F. Larsson, K.-R. Riemschneider, L.E. Asp, Experimental and computational characterization of carbon fibre based structural battery electrode laminae, *Compos. Sci. Technol.* 220 (2022) 109283.
- [14] J. Xu, Z. Geng, M. Johansen, D. Carlstedt, S. Duan, T. Thiringer, F. Liu, L.E. Asp, A multicell structural battery composite laminate, *EcoMat* 4 (3) (2022) e12180.
- [15] J. Xu, C. Creighton, M. Johansen, F. Liu, S. Duan, D. Carlstedt, P. Mota-Santiago, P. Lynch, L.E. Asp, Effect of tension during stabilization on carbon fiber multifunctionality for structural battery composites, *Carbon N Y* 209 (2023) 117982.
- [16] M.S. Siraj, S. Tasneem, D. Carlstedt, S. Duan, M. Johansen, C. Larsson, J. Xu, F. Liu, F. Edgren, L.E. Asp, Advancing structural battery composites: robust manufacturing for enhanced and consistent multifunctional performance, *Adv. Energ. Sust. Res.* 4 (11) (2023) 2300109.
- [17] D. Zenkert, R. Harnden, L.E. Asp, G. Lindbergh, M. Johansson, Multifunctional carbon fibre composites using electrochemistry, *Compos. B Eng.* 273 (2024) 111240.
- [18] W. Johannisson, N. Ihrner, D. Zenkert, M. Johansson, D. Carlstedt, L.E. Asp, F. Sieland, Multifunctional performance of a carbon fiber UD lamina electrode for structural batteries, *Compos. Sci. Technol.* 168 (2018) 81–87.
- [19] R. Tavano, J. Xu, C. Creighton, F. Liu, B. Dharmasin, L.C. Henderson, L.E. Asp, Influence of carbonisation temperatures on multifunctional properties of carbon fibres for structural battery applications, *Batter. Supercapacit.* (2024) e202400110.
- [20] R. Chaudhary, J. Xu, Z. Xia, L.E. Asp, Unveiling the Multifunctional Carbon Fibre Structural Battery, *Adv. Mat.* (2024) 2409725.
- [21] S. Matsuo, N.R. Sottos, Single carbon fiber transverse electrical resistivity measurement via the van der Pauw method, *J. Appl. Phys.* 130 (11) (2021) 115105.
- [22] Q. Zhao, K. Zhang, S. Zhu, H. Xu, D. Cao, L. Zhao, R. Zhang, W. Yin, Review on the electrical resistance/conductivity of carbon fiber reinforced polymer, *Appl. Sci.* 9 (11) (2019) 2390.
- [23] R.A. Huggins, Simple method to determine electronic and ionic components of the conductivity in mixed conductors a review, *Ionics (Kiel)* 8 (2002) 300–313.
- [24] S.N. Patel, A.E. Javier, G.M. Stone, S.A. Mullin, N.P. Balsara, Simultaneous conduction of electronic charge and lithium ions in block copolymers, *ACS nano* 6 (2) (2012) 1589–1600.
- [25] S. Vavra, E. Ahlberg, A. Martinelli, Charge transfer and electrical double layer of an amphiphilic protic ionic liquid in bulk and when confined in nanochannels, *Phys. Chem. Chem. Phys.* 24 (39) (2022) 24469–24479.
- [26] S. Wang, D. Chung, Interlaminar interface in carbon fiber polymer-matrix composites, studied by contact electrical resistivity measurement, *Compos. Interfaces* 6 (6) (1998) 497–505.
- [27] H. Lee, M. Yanilmaz, O. Toprakci, K. Fu, X. Zhang, A review of recent developments in membrane separators for rechargeable lithium-ion batteries, *Energy Environ. Sci.* 7 (12) (2014) 3857–3886.
- [28] M. Kirchhöfer, J. Von Zamory, E. Paillard, S. Passerini, Separators for Li-ion and Li-metal battery including ionic liquid based electrolytes based on the TFSI⁻ and FSI⁻ anions, *Int. J. Mol. Sci.* 15 (8) (2014) 14868–14890.
- [29] S. Duan, A.H. Iyer, D. Carlstedt, F. Rittweger, A. Sharits, C. Maddox, K.-R. Riemschneider, D. Mollenhauer, M. Colliander, F. Liu, et al., Effect of lithiation on the elastic moduli of carbon fibres, *Carbon N Y* 185 (2021) 234–241.
- [30] C. Larsson, F. Larsson, J. Xu, K. Runesson, L.E. Asp, Effects of lithium insertion induced swelling of a structural battery negative electrode, *Compos. Sci. Technol.* 244 (2023) 110299.